Impact of hydration and temperature history on the structure and dynamics of lignin

Journal:	*Green Chemistry*
Manuscript ID	GC-ART-12-2017-003796.R1
Article Type:	Paper
Date Submitted by the Author:	24-Feb-2018

Complete List of Authors:	VURAL, DERYA; Giresun University, Physics Department Gainaru, Catalin; Technische Universität Dortmund, Fakultät Physik O'Neill, Hugh; Oak Ridge National Laboratory, Biology and Soft Matter Division Pu, Yunqiao; Oak Ridge National Laboratory, Joint Institute of Biological Sciences, Biosciences Division Smith, Micholas; UT/ORNL Center for Molecular Biophysics, Parks, Jerry; Oak Ridge National Laboratory, UT/ORNL Center for Molecular Biophysics Pingali, Sai Venkatesh; Oak Ridge National Laboratory, Biology and Soft Matter Division Mamontov, Eugene; Oak Ridge National Laboratory, Chemical and Engineering Materials Division Davison, Brian; Oak Ridge National Laboratory, Biosciences Division Sokolov, Alexei; Oak Ridge National Laboratory, Chemical Sciences Division Ragauskas, Arthur; University of Tennessee, Department of Chemical & Biomolecular Engineering Smith, Jeremy; Oak Ridge National Laboratory, UT/ORNL Center for Molecular Biophysics Petridis, Loukas; Oak Ridge National Laboratory, Center for Molecular Biophyscis

SCHOLARONE™
Manuscripts

Please do not adjust margins

Green Chemistry

ARTICLE

Impact of hydration and temperature history on the structure and dynamics of lignin

Received 00th January 20xx,
Accepted 00th January 20xx

DOI: 10.1039/x0xx00000x

www.rsc.org/

Derya Vural,[abc] Catalin Gainaru,[d] Hugh O'Neill,[ce] Yunquiao Pu,[f] Micholas Dean Smith,[ac] Jerry M. Parks,[ac] Sai Venkatesh Pingali,[e] Eugene Mamontov,[g] Brian H. Davison,[f] Alexei P. Sokolov,[h] Arthur J. Ragauskas,[fi] Jeremy C. Smith,[ac] Loukas Petridis*[ac].

The full utilization of plant biomass for the production of energy and novel materials often involves high temperature treatment. Examples include melt spinning of lignin for manufacturing low-cost carbon fiber and the relocalization of lignin to increase the accessibility of cellulose for production of biofuels. These temperature-induced effects arise from poorly understood changes in lignin flexibility. Here, we combine molecular dynamics simulations with neutron scattering and dielectric spectroscopy experiments to probe the dependence of lignin dynamics on hydration and thermal history. We find a dynamical and structural hysteresis: at a given temperature, the lignin molecules are more expanded and their dynamics faster when the lignin is cooled than when heated. The structural hysteresis is more pronounced for dry lignin. The difference in dynamics, however, follows a different trend, it is found to be more significant at high temperatures and high hydration levels. The simulations also reveal syringyl units to be more dynamic than guiacyl. The results provide an atomic-detailed description of lignin dynamics, important for understanding lignin role in plant cell wall mechanics and for rationally improving lignin processing. The lignin glass transition, at which the polymer softens, is lower when lignin is cooled than when heated, therefore extending the cooling phase of processing and shortening the heating phase may offer ways to lower processing costs.

[This manuscript has been authored by UT-Battelle, LLC under Contract No. DE-AC05-00OR22725 with the U.S. Department of Energy. The United States Government retains and the publisher, by accepting the article for publication, acknowledges that the United States Government retains a non-exclusive, paid-up, irrevocable, world-wide license to publish or reproduce the published form of this manuscript, or allow others to do so, for United States Government purposes. The Department of Energy will provide public access to these results of federally sponsored research in accordance with the DOE Public Access Plan (http://energy.gov/downloads/doe-public-access-plan).]

Introduction

The development of biorefineries, converting whole plant biomass to fuels and chemicals, is a pressing challenge as this would help address the need for renewable energy and reduce CO_2 emissions.[1] Lignin, a major biomass component and the most abundant aromatic polymer in nature, poses both great challenges[2, 3] and opportunities[4, 5] towards this goal. High temperature treatment to disrupt lignin is key to full biomass utilization. Thermochemical pretreatment delocalizes or removes lignin from biomass;[6-13] which serves to enhance biofuel production, as the presence of lignin hinders the efficient hydrolysis of cellulose to sugars for conversion to bioethanol.[3, 14-16] The use of lignin as a precursor for high-value materials, such as carbon fibers,[17-19] plastics[20-23] and films,[24] also requires thermal treatment, both for the isolation of lignin from biomass and for its processing.

At room temperature lignin is mechanically rigid, a state that supports its function in providing mechanical strength to plants, but impedes processing for industrial applications. High temperature is employed to 'soften' lignin. At the molecular scale this is achieved by enhancing the underlying atomic dynamics, resulting in desirable macroscopic changes, such as its redistribution in biomass facilitating biofuel production[15] and molecular flow and orientation for melt-spinning for carbon fiber production.[18]

[a] UT/ORNL Center for Molecular Biophysics, Oak Ridge National Laboratory, Oak Ridge, TN 37831, USA.
[b] Department of Physics, Giresun University, Giresun. Turkey, 28200.
[c] Department of Biochemistry and Cellular and Molecular Biology, University of Tennessee, Knoxville, TN 37996, USA.
[d] Fakultät Physik, Technische Universität Dortmund, 44221 Dortmund, Germany
[e] Biology and Soft Matter Division, Oak Ridge National Laboratory, Oak Ridge, Tennessee 37831, USA
[f] Biosciences Division, Oak Ridge National Laboratory, Oak Ridge, TN 37830, USA
[g] Chemical and Engineering Materials Division, Oak Ridge National Laboratory, Oak Ridge, Tennessee 37831, USA
[h] Chemical Sciences Division, Oak Ridge National Laboratory, Oak Ridge, Tennessee 37831, USA
[i] Department of Chemical & Biomolecular Engineering, University of Tennessee Knoxville, Knoxville, TN 37996, USA
† Footnotes relating to the title and/or authors should appear here.
Electronic Supplementary Information (ESI) available: [details of any supplementary information available should be included here]. See DOI: 10.1039/x0xx00000x

Please do not adjust margins

The temperature-dependent transition, termed the 'glass transition', is common in amorphous polymers. At temperatures below the glass transition temperature (T_g), a polymer is glassy and hard/stiff, whereas above T_g its stiffness decreases considerably and the material may exhibit rubbery behavior.[25] The transition is manifested as an abrupt change in physical properties, *e.g.* the tensile strength, heat capacity and thermal expansion coefficient.[25] For dry lignin, T_g=50-150 °C, depending on the plant source material, the processing conditions, and the method used for measurement.[26, 27]

Lignin is found in environments that contain different amount of water. Secondary cell walls of plants, the native environment of lignin, contain about 30% water on average.[28] After lignin is isolated from plants, it is found in a powder form that is usually in contact with air humidity. When the powder is heated above 100 °C for processing, water evaporates and lignin becomes dry. Hydration reduces the lignin T_g; for example, isolated lignin obtained by acid hydrolysis of softwood has its T_g reduced from 150 to 60 °C when its water content (mass of water/mass of dry lignin) increases from 0 to 18%. [29]

A molecular-level description of the temperature dependence of lignin structure and dynamics is lacking and is, for the reasons above, clearly of practical importance. Here, we employ molecular dynamics (MD) simulations, neutron scattering and dielectric spectroscopy to investigate the variation of lignin dynamics with temperature and hydration during a heating-cooling temperature cycle. We study lignin isolated from the stems of vanilla plants because experimental data exist of its chemical composition that are required to build atomistic models of the polymer.[30] The lignin is found to exhibit both dynamical and structural hysteresis. When measured at the same temperature, heated lignin is less dynamic, *i.e.* exhibits smaller-amplitude atomic motions, and has a smaller size than when cooled down from higher temperature. The magnitude of this dynamical hysteresis increases with hydration, implying that lignin becomes softer in a water-rich environment, such as thermochemical pretreatment of biomass. These results highlight and provide atomic-detailed insight into the dependence of lignin dynamics on processing conditions.

Experimental

Sample Preparation. The lignin from vanilla stems was isolated according to the methods largely described previously.[30, 31] Briefly, the vanilla stems were successively extracted with ethanol:toluene mixture (1:2, v:v) for 24 h and then acetone for additional 12 h. The extractives-free vanilla stems were ball-milled (580 rpm, 5-min pauses in-between for 1.5 h total time) by using a Retsch PM100 ball-mill with a ZrO_2 vessel containing 10 ZrO_2 ball bearings. The ball-milled powder was then subjected to enzymatic hydrolysis in the sodium acetate buffer solution (pH 4.8) at 50°C under continuous agitation at 200 rpm for 48 h. The residual solids were isolated by centrifugation and hydrolyzed one more time with freshly added enzyme mixture. The cellulase treated residues were washed with deionized water, centrifuged, and freeze-dried. The residue was then extracted with dioxane-water (96% v/v, 10.0 mL/g biomass) for 24 h. The extracted mixture was centrifuged and the supernatant was collected. Dioxane extraction was repeated once with the fresh dioxane-water. The combined supernatant was concentrated with a rotary evaporator at ~45°C and then freeze dried. The obtained lignin powder samples were used for dielectric spectroscopy measurements. For the QENS measurements, the lignin was dried in a vacuum oven overnight and sealed in aluminum cans (3 x 5 cm) in a dry glove bag.

Broadband Dielectric Spectroscopy. The dielectric response of lignin was measured at Oak Ridge National Laboratory in the frequency range of 10^{-1} – 10^{6} Hz using a Novocontrol equipment that includes an Alpha-A impedance analyzer and a Quatro temperature control unit. The sample was placed in a parallel-plate dielectric cell similar to the one described in Ref.[32] . Since the material was provided as a powder the precise value of the filling factor could not be estimated. Consequently, the dielectric responses of lignin are presented in Figures S-1 and S-2 (in the Electronic Supporting Information) in arbitrary units.

Neutron Scattering. Elastic intensity scan data were obtained from quasi-elastic neutron scattering (QENS) spectra were collected for dry vanilla lignin at the BASIS spectrometer at Oak Ridge National Laboratory,[33] with an energy resolution (half-width half-maximum) W = 1.7μeV. Two elastic scans were performed in the Q-range 0.3 − 1.9 $Å^{-1}$. In the first, data were collected as the sample was heated from T = 20 − 400 K. The sample was then cooled to 20 K relatively quickly (thus data were not recorded) and data were collected during a second heating phase from T = 20 − 400 K. Due to the incoherent scattering cross section of hydrogen being 10 - 20 times larger than that of other nuclei, the data are dominated by the ps-ns motions of lignin non-exchangeable hydrogen atoms. The analysis of the experiments is described below, see Neutron Scattering Functions.

Computational Models. Structural models of individual lignin molecules were built by using available NMR information on the average chemical composition of stem vanilla lignin.[30] Four different lignin polymers were generated. Each polymer, with a molecular weight of 5 kDa, comprised 16 guaiacyl (G) and six syringyl (S) units and the average linkage composition was β−O−4' 76%, β−5 19% and β−β 5%. The primary structures of each polymer are different from each other, but consistent with the average chemical composition of lignin in vanilla stems. The primary sequence of each lignin can be found in Table S-1 to S-4.

The four lignin polymers were packed in a simulation box of dimensions 35 Å × 38 Å × 30 Å (Figure 1). Three models were prepared with different hydration levels. The first sample is dry, the second is solvated by 56 water molecules and the third is solvated by 276 water molecules, which are corresponding to a hydration levels h = 0.00, 0.05 and 0.25

This journal is © The Royal Society of Chemistry 20xx

grams of water per gram of lignin, respectively. The box was replicated using periodic boundary conditions to mimic the environment of the experimental powder sample. This approach to simulate a powder environment, which maintains nanoscale continuity by packing multiple biomolecules in a periodic simulation box, has been employed successfully (as judged by comparison to experimental results) in numerous studies of proteins [34 35 36 37 38 39 40], RNA [41] and cellulose [42 43]

Molecular Dynamics Simulation. MD simulations were performed with the NAMD 2.11 software.[44] The CHARMM force field for lignin[45] and the TIP3P water model[46] were used. The Particle Mesh Ewald method[47] was used with a grid spacing of 1 Å and a force-switching function to smoothly transition Leonard Jones forces to zero over the range of 10 – 11 Å. Multiple time steps were used: 2 fs for bonded and short-range non-bond forces and 4 fs for long-range electrostatic forces. The cutoff distance for nearest neighbors was 11 Å. The neighbor list was updated every 20 steps with a pair-list distance of 12.5 Å. Constant temperature was maintained by using the Langevin dynamics algorithm with a damping coefficient of 5 ps^{-1}. The pressure was maintained at 1 bar using the Nose-Hoover Langevin piston algorithm[48] that employed a piston oscillation period of 200 fs and a piston damping decay time of 100 fs. The coordinates were saved every 1 fs. All calculations were performed on the Edison supercomputer at NERSC.

The systems were subject to heating and cooling cycles. First, in the 'heating' simulations, the system is heated to 25 independent temperatures T, where T ranges from 150 K to 400 K in 10 K increments. The simulation temperature is then held constant at T for 150 ns. The system is then heated to 600 K for 150 ns and 25 new 'cooling' simulations were performed at temperatures T=(400, 390, 380, ..., 150 K). Analysis was performed using the last 75 ns of the trajectories employing GROMACS[49] and VMD.[50]

Neutron Scattering Functions. Elastic intensity data were obtained from neutron scattering experiments by probing specifically the elastic component (ω=0) of the experimentally accessible resolution broadened dynamic structure factor $S_R(Q,\omega)$, which is the convolution of the incoherent dynamic structure factor S(Q,ω) and the resolution function of the instruments H(ω)

$$S_R(Q,\omega) = \int_{-\infty}^{+\infty} d\omega' S(Q,\omega') H(\omega-\omega'), \quad (1)$$

where S(Q,ω) is the Fourier transform of *I(Q,t)*, defined as:

$$I(Q,t) = \frac{1}{N}\sum_{k=1}^{N} {b_k}^2 \langle e^{-iQ[r_k(t)-r_k(0)]}\rangle, \quad (2)$$

where *Q* is the scattering vector, *N* the number of atoms, b_k and $r_k(t)$ are the incoherent scattering length and the position of atom *k* at a time *t*, respectively.

I(Q,t) was calculated from the MD, which tracks all atomic positions *r(t),* using the SASSENA software[51] (Figures S-3 to S-8). To directly compare the experimental data to the MD simulation, the simulation-derived $S_R(Q,\omega)$ was obtained by multiplying *I(Q,t)* with a Gaussian resolution function and taking the time Fourier transform (Figure S-9):

$$S_R(Q,\omega) = \frac{1}{2\pi}\int_{-\infty}^{+\infty} dt \exp(i\omega t)\, I(Q,t) H(t) = \frac{1}{2\pi}\int_{-\infty}^{+\infty} dt \exp(i\omega t)\, I(Q,t) \exp\left(\frac{-t^2}{2\tau_R}\right), \quad (3)$$

where $\tau_R = (8ln2)^{1/2}\hbar/W$, and the energy resolution width for BASIS is W = 1.7 μeV. In both experimental and MD simulation, the elastic intensity, $S_R(Q,\omega=0)$, was obtained from the area under $S_R(Q,\omega)$ for $|\omega| < W/\hbar \approx 0.0025$ ps^{-1}, *i.e.* inside the energy resolution (see dashed lines in Figure S-9). The MSD is derived from $S_R(Q,\omega=0)$ by employing the Gaussian approximation:[52]

$$MSD = -6\frac{dlnS_R(Q,\omega=0)}{dQ^2} \quad (4)$$

The above analysis was performed for both the experimentally-measured and simulation-derived $S_R(Q,\omega=0)$, see Figure S-10.

Results

We investigate the dynamics of lignin on the *ps* to *ns* timescale and how they are influenced by temperature, hydration and thermal history. MD simulations were conducted at three hydration levels, of 0.00, 0.05 and 0.25 g of water per g of lignin, to approximately reflect the hydration levels of lignin in, dry powder, powder exposed to humidity, and in secondary plant cell walls, respectively. The systems were first heated from 150 K to 600 K (termed 'heating') and subsequently cooled to 150 K (termed 'cooling').

A detailed characterization of the atomic motions of lignin is provided by the incoherent intermediate scattering function *I(Q,t)* in Eq. 2. *I(Q,t)* is a self-correlation function of the positions of the lignin atoms: the faster its decay with time the more dynamic and mobile the atoms are. The relaxation in *I(Q,t),* as shown in Figure 2, is either protracted, *e.g.* for 0% hydration, signaling confined dynamics in what is often termed a secondary ('beta') relaxation, or decays to 0 at long times, e.g. 25% hydration at 400 K, signaling large-scale restructuring motions, often called 'alpha' or structural relaxation.[53, 54]

Three general trends are observed in the calculated *I(Q,t)* in Figure 2: (i) With increasing temperature, *I(Q,t)* decays faster in all models, indicating lignin becomes more dynamic. (ii) The 0% and 5% hydration data are similar to each other, apart from the 400 K cooling simulation, whereas the 25% hydration models have steeper decays. This shows that hydration levels greater than 5% enhance lignin dynamics[55, 56], similar to what has been previously found for cellulose[42] and globular proteins.[34, 37, 57] (iii) At high temperatures (400 K) and

hydration (5% and 25%) *I(Q,t)* decays faster in the cooling compared to the heating simulations. Thermal history thus affects lignin nanosecond dynamics as the polymer is found to be more dynamic when cooled. Importantly, the significantly-enhanced decay of three models at 400 K (5%-cooling, 25%-cooling and 25%-heating) is a signature of fluid-like behavior exhibited at temperatures above the T_g. The above suggest that both hydration and temperature history affect the lignin dynamics.

Many environmental factors may influence the dynamics of lignin: hydration, pH ionic strength and others. Here, we vary only one environmental condition, the hydration content of lignin, while keeping all others constant. Additional studies are needed to assess the effects of other environmental factors that may be important in the pretreatment of biomass and to determine their influence of lignin dynamics

The temperature dependence of lignin dynamics was also studied with dielectric spectroscopy (DS), which probes the reorientational motions of dipoles, i.e. hydroxyl groups in the case of lignin. Analysis of the dielectric spectra of lignin reveals the presence of two relaxation processes below T_g (Figures S-1 and S-2): one is related to the presence of water because it disappears after the sample is heated, while the second process is a genuine relaxation of lignin. The relaxation time of the lignin process, τ, estimated from the frequency of the maximum of the dielectric loss spectra, displays an Arrhenius temperature dependence (Figure 3), $\tau = \tau_0 \exp(E_A/k_B T)$, where τ_0 is a reference relaxation time and E_A=7.65±0.2 kcal/mol is the activation energy associated with this process. Arrhenius behavior is typical of a secondary relaxation in polymers and indicates a simple physical picture: lignin local motions involve transitions between conformational states separated by an average energy barrier E_A in the temperature-invariant underlying energy landscape.

Relaxation times τ were also determined from the MD simulations (0%-cooling, to match the experimental conditions) by fitting a stretched exponential function $I(Q,t) = H + A\, exp\left[-(t/\tau)^{\beta}\right]$ to *I(Q,t)*. Extrapolating the Arrhenius fit of the experimental data to higher temperatures yields good agreement with the simulation-derived relaxation times (Figures 3 and S-11).

The lignin atomic mean-square displacement (MSD), a quantitative measure of the average amplitude of atomic motions, was obtained from quasi-elastic neutron scattering (QENS) experiments performed on dry lignin (Figure 4). Data recorded at two consecutive heating cycles are similar. In both cases, below ~100-150 K the MSD increases linearly with temperature, indicating vibrational motions. At ~ 100-150 K the slope increases due to thermally activated anharmonic motions of the lignin hydrogen atoms; a similar transition temperature is found in the activation of hydrophobic and aromatic protein residues[58]. However, above 150 K lignin MSD increases monotonically, lacking an abrupt transition, a clear indication that the dry polymer does not undergo a glass transition at temperatures less than 400 K.

A direct comparison of experiment and theory is possible by obtaining a simulation-derived MSD the same way as done in experiments: by calculating the QENS elastic intensity, as given by the Fourier transform of *I(Q,t)*, and fitting its *Q*-dependence employing the Gaussian approximation[52] (see Methods and Figures S-9 and S-10). Excellent quantitative agreement is found between the calculated and experimental MSD of dry lignin (Figures 4 and S-12). Similar to *I(Q,t)*, the MSD also displays hysteresis, with hydrated lignin in the cooling simulations found to have larger MSD at high temperatures than the heating simulations. The magnitude of the difference in the MSD between cooling and heating depends on hydration and temperature: it is insignificant for 0% hydration, but becomes very pronounced for 5% and 25% hydration levels at ~400 K and ~380 K, respectively. In the latter case, the jump in MSD is ~10 Å^2, which is comparable to the squared radius of gyration of a lignin unit (12 Å^2), thus indicating that units slide past each other and the polymer becomes softer. The observed hysteresis is similar to the asymmetry in recovery – the phenomenon observed in synthetic polymers at temperatures below T_g.[59] In that case also the recovery (relaxation) is faster when a polymer is cooled down from higher temperature and is slower when heated to the same temperature. This analogy indicates that the simulations reflect aging phenomena below the T_g of lignin.

The nature of lignin atomic motions on the *ps* to *ns* timescale is further characterized by the time-dependent mean square displacement (Figure 5):

$$\langle u^2(t)\rangle = \langle [r(t) - r(0)]^2 \rangle \,. \quad (5)$$

Unlike the MSD of Figure 4 and Equation 4, $\langle u^2 \rangle$ is calculated directly from the atomic positions *r(t)* in the MD trajectories. In the short timescale regime (t < 10-30 ps), all simulations display an initial increase in $\langle u^2 \rangle$ that scales with time as ~$t^{0.25}$. For free diffusion, the exponent is equal to 1, therefore the smaller exponent found here reflects a temporary confinement of lignin atoms. At longer timescales, the six simulation sets differentiate and, similar to Figures 2 and 4, fall in two classes. The 0%-heating, 0%-cooling and the 5%-heating simulations exhibit a plateau in $\langle u^2 \rangle$, in which the average atomic fluctuations do not increase appreciably with time. Lignin units/monomers are constrained by a 'cage' formed by their neighbors, a behavior typical of glassy polymers (Figure 6)[60]. The size of the cage, indicated by the value of $\langle u^2 \rangle$ at the plateau, becomes larger with temperature, but the lignin units remain trapped in it. In contrast, the 5%-cooling, 25%-heating and 25%-cooling simulations do not exhibit a plateau in $\langle u^2 \rangle$. In these cases the lignin units escape their cages (Figure 6), which requires collective motions of a unit and its neighbors, and the time-dependence of $\langle u^2 \rangle$ scales as ~$t^{0.5}$, indicative of sub-diffusive translational motion of the units consistent with the Rouse model, which describes the dynamics of linear, unentangled, ideal ('Gaussian') chains under melt conditions.[61] Chain entanglement and branching, which may occur in lignin, would lead to a weaker time-dependence: ~t^b, with exponent b<0.5.

Figures 2-5 represent the average motions of lignin atoms. We now use the MD simulations, which have been validated

This journal is © The Royal Society of Chemistry 20xx

by the comparison to the DS and QENS experiments, to investigate the contributions made by different functional groups. The lignin polymer contains guaiacyl (G) and syringyl (S) units, which differ in their degree of methoxylation of the phenolic ring. Below T_g, the time-dependent mean square displacement calculated for different units reveals the S units to be more dynamic, *i.e.* have larger $\langle u^2 \rangle$, than G units are (Figures 7 and S-13). The inclusion of the more mobile S units would therefore reduce the T_g of lignin, consistent with previous experiments that have found lignin with a high S/G ratio to have lower T_g.[19, 62] Above T_g both units have similar $\langle u^2 \rangle$, dominated by their translational motions, that are similar between all units because of chain connectivity.

To further examine the difference between S and G dynamics we conducted MD cooling and heating simulations of 0% hydrated S-only and G-only lignin, with the linkage composition and degree of polymerization being the same in the two simulations. As shown in SI Figure S-14, lignin consisting of only S units has larger MSD and its I(Q,t) decays faster than G-only lignin, confirming that S lignin is indeed more dynamic than G. This is explained by the methoxy atoms of lignin found here being more dynamic than non-methoxy atoms. Therefore, the extra methoxy group renders S units more dynamic than G units.

Lignin units can be considered to be made of two chemical moieties, a phenolic ring and a three-carbon aliphatic chain. At short timescales, rings are found to exhibit larger amplitude motions (Figures 7 and S-15). However, at longer timescales (above a 'cross-over' time) tails become more dynamic. The cross-over time is found to decrease with temperature and hydration. Orientational dynamics of the rings are important because their alignment along the lignin carbon fiber axes may be responsible for the desirable high tensile strength of the material. We find that, above T_g, ring orientational dynamics are slower than translational dynamics and that orientational dynamics of rings are faster than those of the tails (Figure S-16).

Finally, to probe whether the temperature history of lignin affects its structure, in addition to its dynamics, we calculated the average radius of gyration (R_g) of a lignin polymer (Figure 8). In the 0% hydration, the R_g in the cooling process is greater than in the heating. This can be understood using both thermodynamic and dynamic considerations. Generally, lignin molecules can exist in collapsed conformations with small R_g or as coils with larger R_g. For dry lignin, the thermodynamically lowest energy state is the latter. However, in a (dry) powder form, lignin molecules are initially in a metastable collapsed state. Although a transition to a coil conformation, which involves significant structural rearrangements, is energetically always favored, at temperatures below T_g the transition is too slow to be observed on the laboratory timescale due to the very slow dynamics in the glassy state. During the heating simulations, the lignin molecules start from a collapsed conformation and remain in it until the simulation temperature exceeds T_g, which is higher than 400 K here. The cooling simulations, however, start from the 600 K, well above T_g, in which the lignin molecules have relaxed to the equilibrium coil conformation that has a larger R_g and maintain those conformations for all temperatures. The hysteresis is thus explained by lignin being 'frozen' in metastable collapsed states during the heating simulations.

The presence of water, which is a 'poor' solvent of lignin, changes the thermodynamics of the lignin conformations. The compact states are energetically favored, to minimize lignin-water interactions.[56, 63] Unlike the dry systems, the R_g of lignin is similar for both heating and cooling processes (Figure S-17). Hysteresis in the R_g therefore depends on the amount of water in the model, decreasing with hydration.

Conclusions

Lignin is of central importance in the utilization of plant biomass as an abundant, renewable source material for the production of biofuels and bioproducts. The valorization of lignin has involved temperature treatments to make it softer. To obtain an atomic-detail description of the dynamics as lignin is heated and cooled, we employ MD simulations, validated by quantitative and direct comparison to neutron scattering and dielectric spectroscopy experiments. We examined three water levels, approximately corresponding to that in the plant cell wall (25% w/w) and of isolated powder lignin (5% and 0% w/w). We found a dynamical hysteresis for hydrated lignin: at each temperature lignin exhibits faster dynamics when cooled to this temperature than when heated. The magnitude of this hysteresis depends on the hydration level of lignin. At 0% water, the difference between heating and cooling simulations is negligible: both exhibit local dynamics, in which lignin units are trapped by a 'cage' formed by its neighbors and cannot slide past each other. On the other hand, at 5% water content the heating and cooling simulations display markedly different behavior. The former shows local dynamics, similar to the 0% dry samples, but in the latter units escape their 'cage' and display long range translational motions, a signature that lignin has crossed over from a glassy to a soft state.

The transition to non-local dynamics that make lignin softer is critical to its processing. We show here that the transition temperature decreases with hydration, found to be lowest (380 K) in cooling simulations at hydration levels comparable to the plant cell wall (25% g water / g lignin). Once extracted, lignin, which is in a powder form hydrated by moisture, has a slightly higher T_g (400 K). When all moisture is removed by heating and the powder becomes dry, lignin T_g increases further to temperatures higher than those examined here (> 400 K). Thus, the incremental removal of water as lignin is being processed, from plant cell walls to dry powder, necessitates higher temperatures to soften lignin.

The above insights may guide more efficient lignin processing conditions that reduce the cost of its transformation to high value products by operating at the lowest necessary temperature. The softening of lignin occurs at lower temperatures when whole biomass is thermochemically pretreated, a process that necessarily includes a relatively high amount of water, than when isolated

powder lignin is heated up. In both cases, the softening temperature is lower when the isolated lignin is cooled than when heated, therefore extending the cooling phase of processing may offer ways to lower the processing cost of lignin.

We examined details of how the chemical composition of lignin affects its dynamics. S units, which contain one more methoxy group, were found to be more dynamic than G units. This is explained by the methoxy groups found to be more dynamin than non-methoxy groups. Lignin can be considered to consist of three-carbon aliphatic chains (tails) and the phenolic rings. At times longer than ~100 ps, tails were found in the simulations to have a larger MSD, i.e. are overall more dynamic, than rings.

Some of the environmental impact of biorefineries comes from the requirement to heat biomass to high temperatures to soften and process lignin. Thus, the use of lower processing temperatures will lead to greener biorefineries. The data we present here suggest two possible ways to reduce the lignin processing temperature: The cooling phase of the processing should be prolonged and heating should be shortened; Feedstocks whose lignin has a higher syringyl content should also be used.

Conflicts of interest

There are no conflicts to declare.

Acknowledgements

This research was supported by the Genomic Science Program, Office of Biological and Environmental Research, U. S. Department of Energy (DOE), under Contract FWP ERKP752. CG and APS acknowledge support by the DOE Office of Science, BES Materials Sciences and Engineering Division for the dielectric studies. This research used resources of the National Energy Research Scientific Computing Center, a DOE Office of Science User Facility supported by the Office of Science of the U.S. Department of Energy under Contract No. DE-AC02-05CH11231. This research used resources at the Spallation Neutron Source, a DOE Office of Science User Facility operated by the Oak Ridge National Laboratory, managed by UT-Battelle, LLC, for DOE under Contract DE-AC05-00OR22725.

This journal is © The Royal Society of Chemistry 20xx

Figures

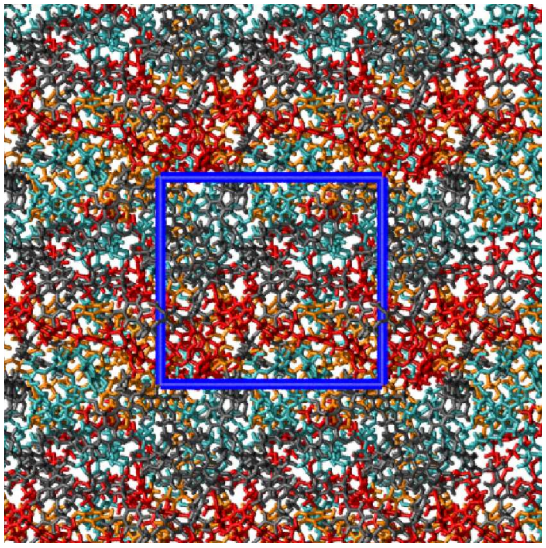

Figure 1: Snapshot of the simulation system, with four lignin molecules (red, orange, grey and cyan) packed in a simulation box (blue) that employs periodic boundary conditions.

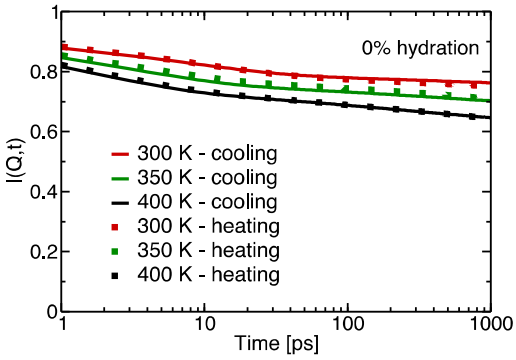

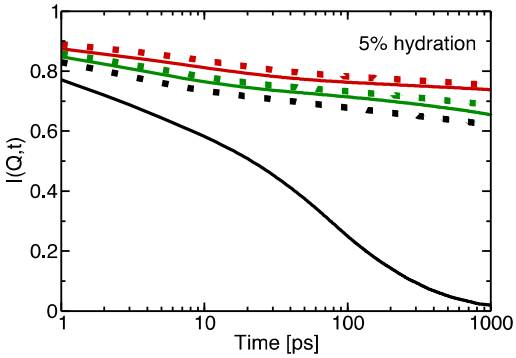

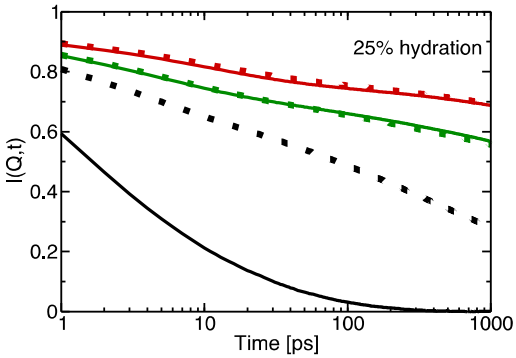

Figure 2: Intermediate scattering function, calculated for the lignin atoms only, as a function of time for wave-vector Q=1.1 $Å^{-1}$ for heating (dotted line) and cooling (solid line) thermal treatments, at 300K (red), 350K (green) and 400 K (black) for three w/w hydration levels 0% (top), 5% (middle) and 25% (bottom). The average nearest neighbor distance between lignin units is ~6 Å (Ref. 56), corresponding to Q=2π/6=1.05 $Å^{-1}$, therefore the wavevector shown here probes motions at inter-unit distances. For the Q dependence of I(Q,t) see Figures S-3 to S-8.

This journal is © The Royal Society of Chemistry 20xx

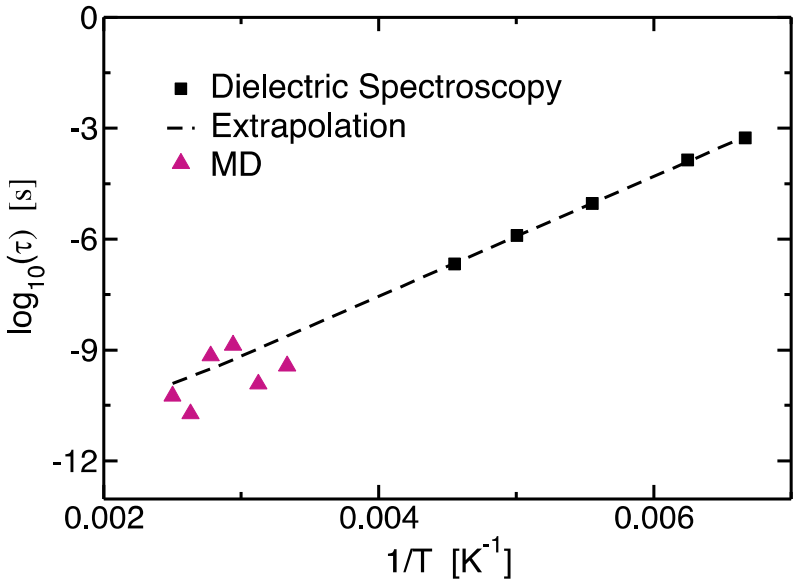

Figure 3: Temperature dependence of the relaxation time obtained from dielectric spectroscopy experiments (squares) and MD simulations (triangles) when 0% hydrated lignin was cooled from 440 K to 150 K. The dotted line is an Arrhenius fit to the experimental data. Fits to the MD data are shown in Figure S-11.

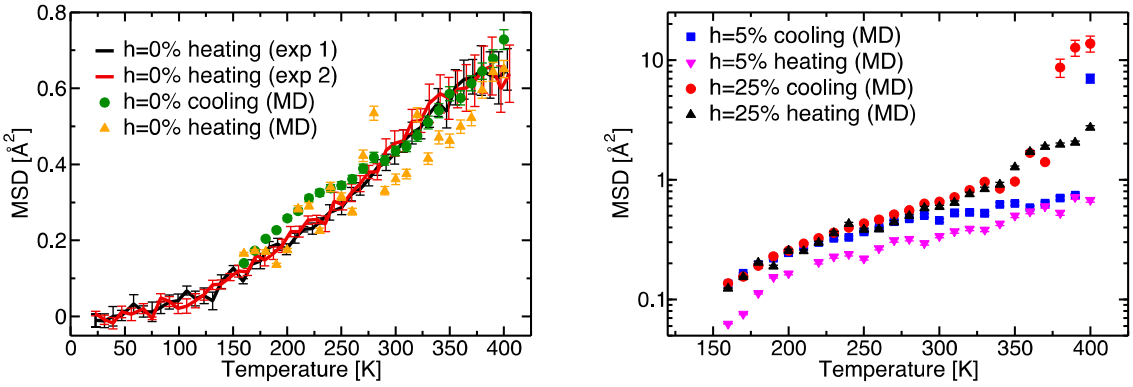

Figure 4: Lignin mean square displacement calculated from the elastic intensity (Eq. 4, Figures S-9 and S-10) plotted as a function of temperature. To allow comparison of simulation and QENS experiment (see also Figure S-12), we plot the MSD relative to that at 150K, the lowest simulation temperature. In the experiments, the samples were heated from 20K to 400 K ('exp 1'), then cooled to 20K and heated again to 400 K ('exp 2'), with data recorded only during the two heating cycles.

This journal is © The Royal Society of Chemistry 20xx

Please do not adjust margins

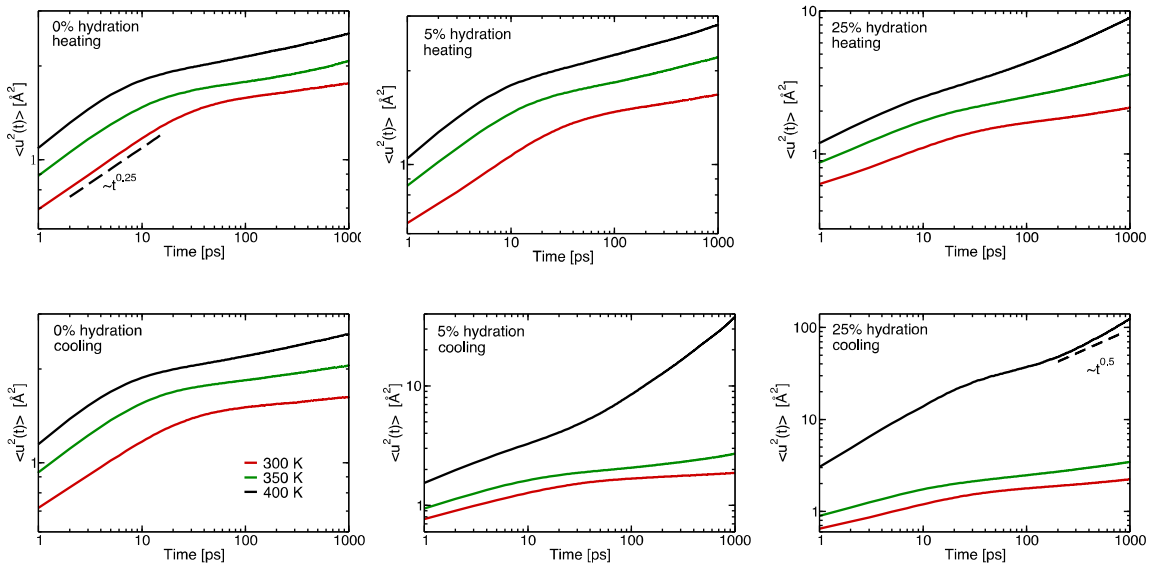

Figure 5: Mean square displacement vs. time calculated from the coordinates of the lignin non-exchangeable hydrogen atoms (Eq. 5) for heating and cooling simulations at three hydration levels, 0, 5 and 25 % g water / g lignin, and three temperatures, 300 (red), 350 (green) and 400 (black) K. The dashed lines represent $\sim t^{0.25}$ and $\sim t^{0.50}$ time dependence.

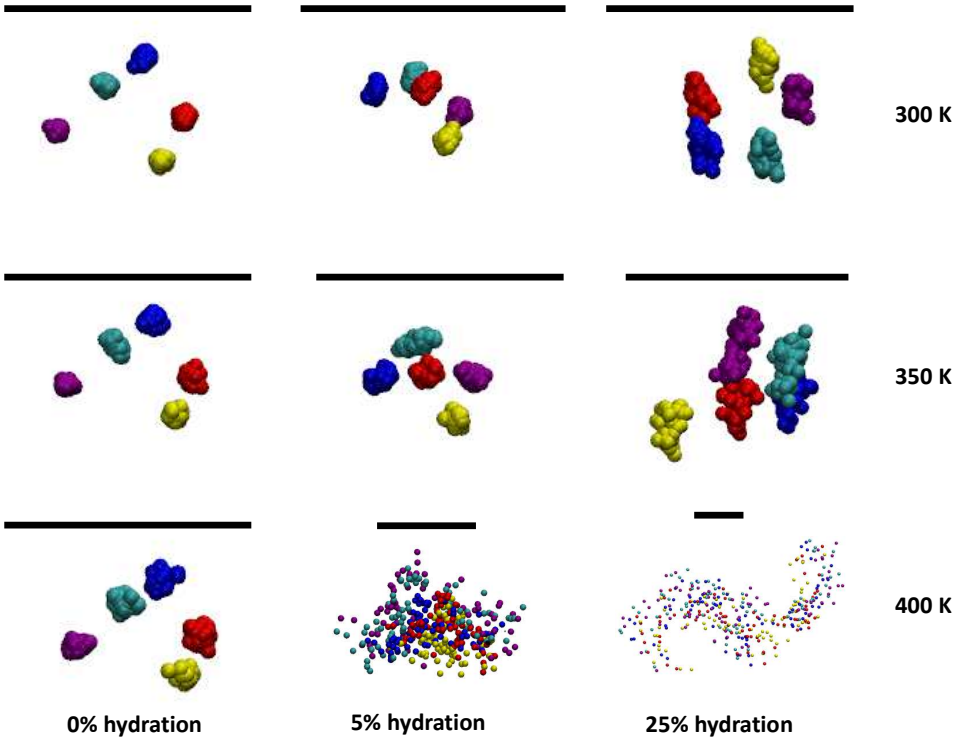

Figure 6: Snapshots of the positions of C1 atoms of five lignin units, taken at 1 ns intervals over the last 75ns of the cooling MD trajectories at 300, 350 and 400 K for at hydration levels, 0, 5 and 25 %. Atoms are coloured according to which unit they belong to. The black lines above each image are 20 Å scale bars.

This journal is © The Royal Society of Chemistry 20xx

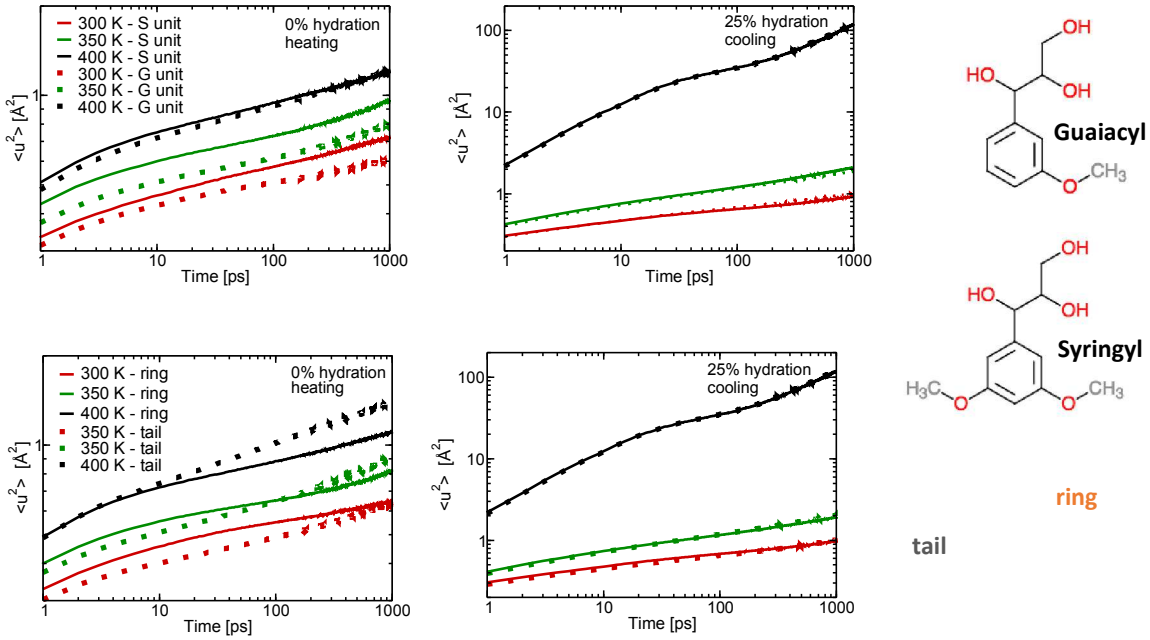

Figure 7: Average time-dependent mean square displacement of guaiacyl (G), syringyl (S), tail and ring atoms. The chemical structure of the units and the decomposition to ring and tail atoms is shown on the right. The data from the other simulations are shown in Figures S-13 to S-16.

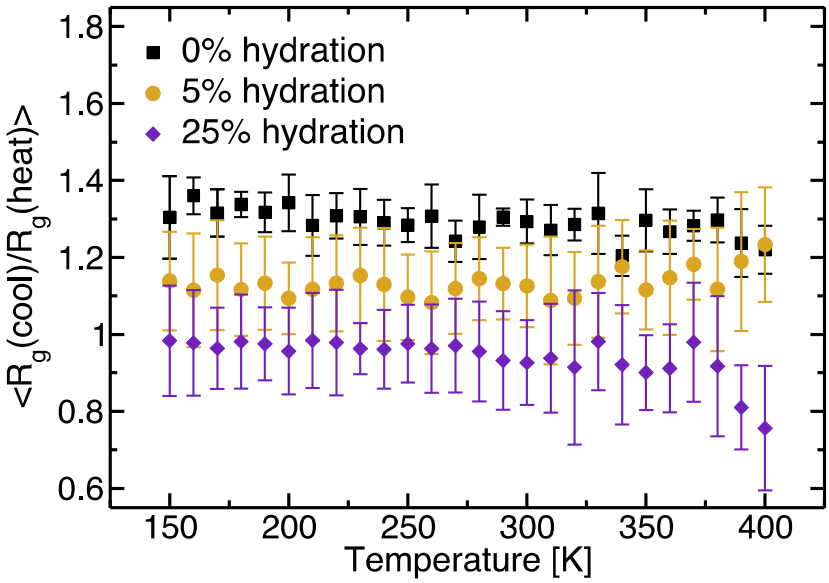

Figure 8: Ratio of the average radius of gyration of a lignin polymer for cooling simulations over that for heating simulations. <> indicate time and ensemble averages. Figure S-17 shows R_g(cool) and R_g(heat).

This journal is © The Royal Society of Chemistry 20xx

Notes and references

1. T. Parsell, S. Yohe, J. Degenstein, T. Jarrell, I. Klein, E. Gencer, B. Hewetson, M. Hurt, J. I. Kim, H. Choudhari, B. Saha, R. Meilan, N. Mosier, F. Ribeiro, W. N. Delgass, C. Chapple, H. I. Kenttamaa, R. Agrawal and M. M. Abu-Omar, *Green Chemistry*, 2015, **17**, 1492-1499.
2. M. E. Himmel, S. Y. Ding, D. K. Johnson, W. S. Adney, M. R. Nimlos, J. W. Brady and T. D. Foust, *Science*, 2007, **315**, 804-807.
3. J. V. Vermaas, L. Petridis, X. Qi, R. Schulz, B. Lindner and J. C. Smith, *Biotechnol. Biofuels*, 2015, **8**, 1-16.
4. A. J. Ragauskas, G. T. Beckham, M. J. Biddy, R. Chandra, F. Chen, M. F. Davis, B. H. Davison, R. A. Dixon, P. Gilna, M. Keller, P. Langan, A. K. Naskar, J. N. Saddler, T. J. Tschaplinski, G. A. Tuskan and C. E. Wyman, *Science*, 2014, **344**, 1246843.
5. Y. Mottiar, R. Vanholme, W. Boerjan, J. Ralph and S. D. Mansfield, *Current Opinion in Biotechnology*, 2016, **37**, 190-200.
6. H. Trajano, N. Engle, M. Foston, A. Ragauskas, T. Tschaplinski and C. Wyman, *Biotechnol. Biofuels*, 2013, **6**, 110.
7. S. P. S. Chundawat, B. S. Donohoe, L. D. Sousa, T. Elder, U. P. Agarwal, F. C. Lu, J. Ralph, M. E. Himmel, V. Balan and B. E. Dale, *Energy & Environmental Science*, 2011, **4**, 973-984.
8. B. S. Donohoe, S. R. Decker, M. P. Tucker, M. E. Himmel and T. B. Vinzant, *Biotechnol. Bioeng.*, 2008, **101**, 913-925.
9. S. Singh, G. Cheng, N. Sathitsuksanoh, D. Wu, P. Varanasi, A. George, V. Balan, X. Gao, R. Kumar, B. E. Dale, C. E. Wyman and B. A. Simmons, *Front, Energy Res,*, 2015, **2**.
10. A. M. Socha, R. Parthasarathi, J. Shi, S. Pattathil, D. Whyte, M. Bergeron, A. George, K. Tran, V. Stavila, S. Venkatachalam, M. G. Hahn, B. A. Simmons and S. Singh, *PNAS*, 2014, **111**, E3587-E3595.
11. L. D. Sousa, M. J. Jin, S. P. S. Chundawat, V. Bokade, X. Y. Tang, A. Azarpira, F. C. Lu, U. Avci, J. Humpula, N. Uppugundla, C. Gunawan, S. Pattathil, A. M. Cheh, N. Kothari, R. Kumar, J. Ralph, M. G. Hahn, C. E. Wyman, S. Singh, B. A. Simmons, B. E. Dale and V. Balan, *Energy & Environmental Science*, 2016, **9**, 1215-1223.
12. F. Xu, J. Sun, N. V. S. N. M. Konda, J. Shi, T. Dutta, C. D. Scown, B. A. Simmons and S. Singh, *Energy & Environmental Science*, 2016, **9**, 1042-1049.
13. P. Langan, L. Petridis, H. M. O'Neill, S. V. Pingali, M. Foston, Y. Nishiyama, R. Schulz, B. Lindner, B. L. Hanson, S. Harton, W. T. Heller, V. Urban, B. R. Evans, S. Gnanakaran, A. J. Ragauskas, J. C. Smith and B. H. Davison, *Green Chem.*, 2014, **16**, 63-68.
14. L. Kumar, V. Arantes, R. Chandra and J. Saddler, *Bioresource Technol.*, 2012, **103**, 201-208.
15. H. J. Li, Y. Q. Pu, R. Kumar, A. J. Ragauskas and C. E. Wyman, *Biotechnol. Bioeng.*, 2014, **111**, 485-492.
16. H. Jorgensen, J. B. Kristensen and C. Felby, *Biofuels Bioprod. Bioref.*, 2007, **1**, 119-134.
17. D. A. Baker and T. G. Rials, *J Appl Polym Sci*, 2013, **130**, 713-728.
18. W. Fang, S. Yang, X. L. Wang, T. Q. Yuan and R. C. Sun, *Green Chemistry*, 2017, **19**, 1794-1827.
19. Q. N. Sun, R. Khunsupat, K. Akato, J. M. Tao, N. Labbe, N. C. Gallego, J. J. Bozell, T. G. Rials, G. A. Tuskan, T. J. Tschaplinski, A. K. Naskar, Y. Q. Pu and A. J. Ragauskas, *Green Chem.*, 2016, **18**, 5015-5024.
20. S. Kubo and J. F. Kadla, *Macromolecules*, 2004, **37**, 6904-6911.
21. H. Y. Chung and N. R. Washburn, *Green Materials*, 2013, **1**, 137-160.
22. T. Bova, C. D. Tran, M. Y. Balakshin, J. Chen, E. A. Capanema and A. K. Naskar, *Green Chem*, 2016, **18**, 5423-5437.
23. S. Zhao and M. M. Abu-Omar, *Macromolecules*, 2017, **50**, 3573-3581.
24. J. Wang, R. Boy, N. A. Nguyen, J. K. Keum, D. A. Cullen, J. Chen, M. Soliman, K. C. Littrell, D. Harper, L. Tetard, T. G. Rials, A. K. Naskar and N. Labbé, *ACS Sustainable Chem. Eng.*, 2017, DOI: 10.1021/acssuschemeng.7b01639.
25. G. M. Irvine, *Wood Science and Technology*, 1985, **19**, 139-149.
26. W. Y. Li, N. Sun, B. Stoner, X. Y. Jiang, X. M. Lu and R. D. Rogers, *Green Chemistry*, 2011, **13**, 2038-2047.
27. H. Hatakeyama and T. Hatakeyama, *Adv Polym Sci*, 2010, **232**, 1-63.
28. D. J. Cosgrove and M. C. Jarvis, *Front. Plant Sci.*, 2012, **3**, 204.
29. H. Hatakeyama, Y. Tsujimoto, M. J. Zarubin, S. M. Krutov and T. Hatakeyama, *J Therm Anal Calorim*, 2010, **101**, 289-295.
30. F. Chen, Y. Tobimatsu, D. Havkin-Frenkel, R. A. Dixon and J. Ralph, *Proc Natl Acad Sci U S A*, 2012, **109**, 1772-1777.
31. Q. N. Sun, Y. Q. Pu, X. Z. Meng, T. Wells and A. J. Ragauskas, *Acs Sustainable Chemistry & Engineering*, 2015, **3**, 2203-2210.
32. H. Wagner and R. Richert, *Journal of Physical Chemistry B*, 1999, **103**, 4071-4077.
33. E. Mamontov and K. W. Herwig, *Rev. Sci. Instrum.*, 2011, **82**.
34. M. Tarek and D. J. Tobias, *Phys. Rev. Lett.*, 2002, **88**.
35. K. Wood, A. Frolich, A. Paciaroni, M. Moulin, M. Hartlein, G. Zaccai, D. J. Tobias and M. Weik, *J. Am. Chem. Soc.*, 2008, **130**, 4586-4587.
36. L. Hong, N. Smolin, B. Lindner, A. P. Sokolov and J. C. Smith, *Phys. Rev. Lett.*, 2011, **107**.
37. J. H. Roh, J. E. Curtis, S. Azzam, V. N. Novikov, I. Peral, Z. Chowdhuri, R. B. Gregory and A. P. Sokolov, *Biophys. J.*, 2006, **91**, 2573-2588.
38. Y. Joti, H. Nakagawa, M. Kataoka and A. Kitao, *Biophysical Journal*, 2008, **94**, 4435-4443.
39. G. Schiro, Y. Fichou, F. X. Gallat, K. Wood, F. Gabel, M. Moulin, M. Hartlein, M. Heyden, J. P. Colletier, A. Orecchini, A. Paciaroni, J. Wuttke, D. J. Tobias and M. Weik, *Nature Communications*, 2015, **6**.
40. Y. Fichou, M. Heyden, G. Zaccai, M. Weik and D. J. Tobias, *Journal of Physical Chemistry B*, 2015, **119**, 12580-12589.
41. G. K. Dhindsa, D. Bhowmik, M. Goswami, H. O'Neill, E. Mamontov, B. G. Sumpter, L. Hong, P. Ganesh and X. Q. Chu, *Journal of Physical Chemistry B*, 2016, **120**, 10059-10068.

42. L. Petridis, H. M. O'Neill, M. Johnsen, B. Fan, R. Schulz, E. Mamontov, J. Maranas, P. Langan and J. C. Smith, *Biomacromolecules*, 2014, **15**, 4152-4159.
43. H. O'Neill, S. V. Pingali, L. Petridis, J. He, E. Mamontov, L. Hong, V. Urban, B. Evans, P. Langan, J. C. Smith and B. H. Davison, *Scientific Reports*, 2017, **7**, 11840.
44. J. C. Phillips, R. Braun, W. Wang, J. Gumbart, E. Tajkhorshid, E. Villa, C. Chipot, R. D. Skeel, L. Kale and K. Schulten, *J. Comput. Chem.*, 2005, **26**, 1781-1802.
45. L. Petridis and J. C. Smith, *J. Comput. Chem.*, 2009, **30**, 457-467.
46. W. L. Jorgensen, J. Chandrasekhar, J. D. Madura, R. W. Impey and M. L. Klein, *J. Chem. Phys.*, 1983, **79**, 926-935.
47. U. Essmann, L. Perera, M. L. Berkowitz, T. Darden, H. Lee and L. G. Pedersen, *J. Chem. Phys.*, 1995, **103**, 8577-8593.
48. G. J. Martyna, D. J. Tobias and M. L. Klein, *J. Chem. Phys.*, 1994, **101**, 4177-4189.
49. M. J. Abraham, T. Murtola, R. Schulz, S. Páll, J. C. Smith, B. Hess and E. Lindahl, *SoftwareX*, 2015, **1–2**, 19-25.
50. W. Humphrey, A. Dalke and K. Schulten, *J. Mol. Graphics*, 1996, **14**, 33-38.
51. B. Lindner and J. C. Smith, *Comput. Phys. Commun.*, 2012, **183**, 1491-1501.
52. A. Rahman, K. S. Singwi and A. Sjölander, *Phys. Rev.*, 1962, **126**, 986-996.
53. C. Bennemann, W. Paul, K. Binder and B. Dünweg, *Phys. Rev. E*, 1998, **57**, 843-851.
54. N. V. Dokholyan, E. Pitard, S. V. Buldyrev and H. E. Stanley, *Phys. Rev. E*, 2002, **65**.
55. L. Petridis, S. V. Pingali, V. Urban, W. T. Heller, H. M. O'Neil, M. Foston, A. Ragauskas and J. C. Smith, *Phys. Rev. E*, 2011, **83**, 061911.
56. L. Petridis, R. Schulz and J. C. Smith, *J. Am. Chem. Soc.*, 2011, **133**, 20277-20287.
57. L. Hong, X. Cheng, D. C. Glass and J. C. Smith, *Phys. Rev. Lett.*, 2012, **108**, 238102.
58. Y. Miao, Z. Yi, D. C. Glass, L. Hong, M. Tyagi, J. Baudry, N. Jain and J. C. Smith, *J. Am. Chem. Soc.*, 2012, **134**, 19576-19579.
59. C. A. Angell, K. L. Ngai, G. B. McKenna, P. F. McMillan and S. W. Martin, *Journal of Applied Physics*, 2000, **88**, 3113-3157.
60. C. Bennemann, W. Paul, K. Binder and B. Dunweg, *Physical Review E*, 1998, **57**, 843-851.
61. M. Doi and S. F. Edwards, *Journal of the Chemical Society-Faraday Transactions Ii*, 1978, **74**, 1789-1801.
62. A. Tejado, C. Pena, J. Labidi, J. M. Echeverria and I. Mondragon, *Bioresource Technology*, 2007, **98**, 1655-1663.
63. L. Petridis and J. C. Smith, *ChemSusChem*, 2016, **9**, 289-295.

This journal is © The Royal Society of Chemistry 20xx